

Facial Action Unit Detection Based on Multi-task Learning Strategy for Unlabeled Facial Images in the Wild

Ziqiao Shang^{a,1}, Bin Liu^{b,*}

^aSchool of Electronic Information and Communications, Huazhong University of Science and Technology (HUST), Wuhan 430074, China

^bSchool of Computing and Artificial Intelligence, Southwest Jiaotong University

ARTICLE INFO

Keywords:

Facial action unit detection
Multi-task learning strategy
Pixel-level feature alignment scheme
Weighted asymmetric loss

ABSTRACT

Facial Action Unit (AU) detection often relies on highly-cost accurate labeling or inaccurate pseudo labeling techniques in recent years. How to introduce large amounts of unlabeled facial images in the wild into supervised AU detection frameworks has become a challenging problem. Additionally, nearly every type of AUs has the problem of unbalanced positive and negative samples. Inspired by other multi-task learning frameworks, we first propose a multi-task learning strategy boosting AU detection in the wild through jointing facial landmark detection and AU domain separation and reconstruction. Our introduced dual domains facial landmark detection framework can solve the lack of accurate facial landmark coordinates during the AU domain separation and reconstruction training process, while the parameters of homostructural facial extraction modules from these two similar facial tasks are shared. Moreover, we propose a pixel-level feature alignment scheme to maintain the consistency of features obtained from two separation and reconstruction processes. Furthermore, a weighted asymmetric loss is proposed to change the contribution of positive and negative samples of each type of AUs to model parameters updating. Experimental results on three widely used benchmarks demonstrate our superiority to most state-of-the-art methods for AU detection.

1. Introduction

Facial Action Coding System (FACS) (Rosenberg and Ekman, 2020) is a widely used method for coding facial expressions. It has proposed a set of 44 facial action units (AUs) that establish a connection between facial muscle movements and facial expressions (Dahmane and Meunier, 2014), allowing for their simulation. In recent years, AU detection (Zhao et al., 2016; Corneanu et al., 2018; Li et al., 2018; Ma et al., 2019) has become a technique that uses computer vision algorithms to automatically detect and track the AUs in videos or images, which is now promising applications in diverse fields, including human-computer interaction (Bauer et al., 2008), emotion analysis (McDuff et al., 2013; Szirtes et al., 2013), and car-driving monitoring (Vicente et al., 2015).

Recently, due to the high labor cost to obtain a large number of high-precision AU labels for images, self-supervised learning has garnered significant attention for AU detection (Wiles et al., 2018a,b; Li et al., 2019; Lu et al., 2020; Sun et al., 2021; Li et al., 2022; Li and Shan, 2023). These methods do not rely on costly manual labeling. However, most self-supervised methods proposed so far mainly concentrate on images in laboratory scene, which have low generalization performance in the wild. Moreover, some semi-supervised and weakly-supervised methods (Wang et al., 2017; Zhao et al., 2018; Niu et al., 2019; Yan et al., 2023; Yang et al., 2023; Liu et al., 2023) are introduced into AU detection, which combine labeled and unlabeled images in

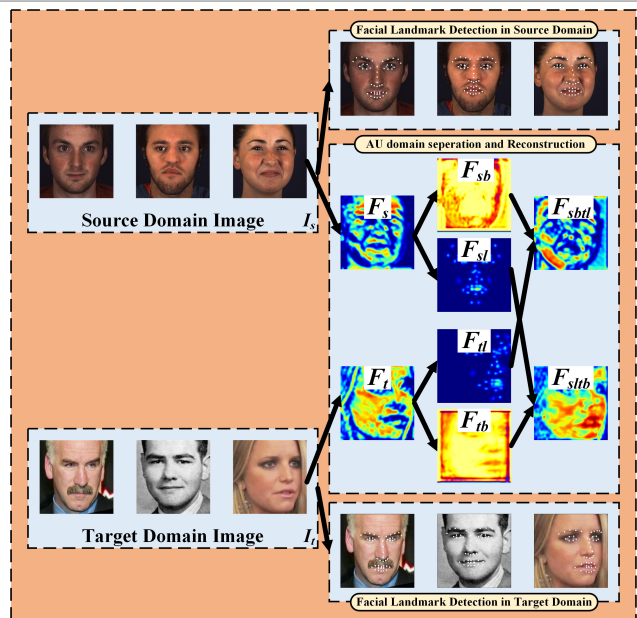


Figure 1: Illustration of jointly learning facial landmark detection with AU domain separation and reconstruction.

training process, and generate pseudo labels through reasoning on unlabeled images. However, the pseudo labels in the wild are also automatically labeled by AU detection frameworks trained in laboratory scene, which can not solve the problem of the large domain distribution difference between annotated images and training images. Comparing images captured in controlled laboratory settings to those taken in the wild, there are notable disparities in various aspects. These disparities encompass variations in facial expressions, poses, ages, lighting conditions, accessories,

*Corresponding author

✉ M202172456@hust.edu.cn (Z. Shang); binliu@swjtu.edu.cn (B. Liu)
ORCID(s): 0009-0006-0468-7497 (Z. Shang); 0000-0002-1011-2909 (B. Liu)

occlusions, backgrounds, and the overall quality of the images. Therefore, how to make AU detection have strong generalization in the wild is a challenging task.

To solve the problem of imprecise pseudo labeling in the wild, we introduce a novel facial task called AU domain feature separation and reconstruction, which can transfer AU knowledge from a source domain in laboratory scene with accurate AU labels to a target domain in the wild without AU labels. One kind of schemes is to learn features that are invariant across different domains (Ganin et al., 2016; Tzeng et al., 2017). However, these approaches may lead to the loss of AU-related information due to the interdependence between AUs and head poses. Another kind of schemes involves transforming source-domain images to resemble the style of the target domain (Lee et al., 2018; Zheng et al., 2018). Nonetheless, these approaches alone may not adequately address other forms of domain shift caused by factors like variations of head poses or facial occlusions. Additionally, Shao et al. (2022) propose to mix facial features from source domain and backgrounds from target domain. This method preserve facial features by accurate facial landmark ground truths. However, it is very unpractical to obtain a large amount of accurate facial landmark ground truths during the training process, especially in target domain.

Due to the similarity in feature extraction for facial tasks, multi-task learning training strategies are widely applied in AU detection (Jyoti et al., 2018; Tallec et al., 2022). These strategies provide more flexible, efficient, and robust ways to learn facial features among different facial tasks, which also help improve the generalization performance of the models extracting facial features. By training on multiple facial tasks, the models can learn richer, generic features that make it better able to adapt to new facial tasks or previously unseen facial images. In previous work (Shao et al., 2021; Wang et al., 2023), facial landmark detection is the most common task combined with AU detection due to the fact that AU centers can be located by the results of facial landmark detection, so as to realize the regional learning of AUs. However, many AU domain separation and reconstruction frameworks also need to use accurate facial landmark coordinates and AU labels, and there is no multi-task learning framework to combine these three tasks together.

Our proposed solutions. Inspired by the above issues, we propose a multi-task learning strategy boosting AU detection in the wild through jointing facial landmark detection and AU domain separation and reconstruction. To make AU detection have strong generalization in the wild, the introduced AU domain separation and reconstruction framework can realize the combination of AU-related features from source domain and background features from target domain. Different from utilizing inaccurate pseudo labels, AU labels from source domain are accurate, and it can also generalize the performance in the wild because of the background features from target domain during the training process. This way not only addresses complex labeling with high labor

cost, but also solve the problem of additional domain shifts arising from head pose variations and occlusions.

Furthermore, the introduced dual domains facial landmark detection framework can enable the framework to use accurate facial landmark coordinates and take advantage of the strong correlation among different facial tasks with similar features. While precise AU ground truths are not accessible for the target domain, our proposed facial landmark framework can generate accurate facial landmark labels highly relevant to AUs. These labels are utilized to predefine AU centers. The facial landmark ground truths for the target domain are readily obtainable through contemporary landmark detection methods (King, 2012; Zhu et al., 2016; Simon et al., 2017; Wu et al., 2018) exhibiting high accuracy comparable to manual labeling. More importantly, our proposed multi-task learning strategy can jointly learn above two facial tasks by sharing the parameters of facial extraction modules with the same structure, which also promotes the precision of AU detection. The learning process of two above facial tasks is illustrated in Fig. 1.

In addition, to maintain the consistency of features obtained from two separation and reconstruction processes, we propose a pixel-level feature alignment scheme, which is realized by projectors with simple structure and an improved self-reconstruction loss. Compared to feature reconstruction processes of other self-supervised frameworks (Shao et al., 2022; Bhattacharya et al., 2020), our framework uses projectors to magnify the receptive field of feature pixel elements to achieve better alignment, and ensures the integrity of the whole reconstruction process by adding four intermediate supervisors, while also increasing the interpretability of the framework. Apart from that, to solve the serious imbalance problem of positive and negative samples of each type of AUs, we propose a weighted asymmetric loss to respectively change the contribution of positive and negative samples to model parameters updating. The main contributions of our work are summarized as follows:

- We propose a multi-task learning strategy boosting AU detection through jointing facial landmark detection and AU domain separation and reconstruction. To our knowledge, this is the first work to jointly learn these two facial tasks for AU detection.
- We propose a pixel-level feature alignment scheme. The simple projectors are developed for magnifying the receptive field of feature pixel elements and an improved self-supervised loss adding four intermediate supervisors is proposed for maintaining the consistency of features obtained from two separation and reconstruction processes.
- We propose a weighted asymmetric loss for respectively changing the contribution of positive and negative samples of each type of AUs to model parameters updating.

- Extensive experiments on three widely-used datasets demonstrate that our method soundly outperforms most state-of-the-art techniques.

2. Related Work

We mainly review three techniques that are most relevant to our work, including self-supervised and semi-supervised AU detection, AU domain separation and reconstruction and multi-task learning frameworks for AU detection.

2.1. Self-supervised and semi-supervised AU detection

Recently, there has been a surge in efforts to enhance the accuracy of AU detection through the application of self-supervised learning. In the field of self-supervised learning for AU detection, extracting supervised knowledge from extensive unlabeled input predominantly necessitates auxiliary tasks (Yan et al., 2021). Wiles et al. (2018a) introduced the Fab-Net, leveraging facial movement transformations between consecutive frames as the supervisory signal to learn facial embedding through reconstruction loss. Inspired by Fab-Net, Li et al. (2019) modified facial actions and head poses to decouple facial features from head posture. However, most of these endeavors focus solely on global facial features, overlooking some AU-related knowledge, such as the distinctive properties of AUs, including locality and relevance. Learning only global features has limited efficacy in AU detection since each AU correlates with specific facial muscles and does not manifest independently.

Additionally, several self-supervised methods have been developed to generate potent visual representations for single-object detection through contrastive learning. Chen et al. (2020) proposed SimCLR, a framework training a base encoder network and a projection to maximize agreement using a contrastive loss. He et al. (2020) introduced MoCo, incorporating a momentum network to store a queue of negative samples for efficient contrastive learning. Lu et al. (2020) utilized temporal consistency for feature representation learning through contrastive learning. Chen and He (2021) achieved general representations without negative sample pairs, avoiding undesired collapsing solutions via a stop-gradient operation. Li and Shan (2023) formulated a contrastive self-supervised learning method for encoding discriminative AU representations from an abundant supply of unlabeled facial videos. However, the prevalent use of self-supervised tasks based on random crops or temporal consistency in contrastive approaches can lead to insufficient AU representations, underutilizing the benefits of static datasets.

Furthermore, the acquisition of reliable AU labels is challenging and highly-cost, and often tainted by noise and errors. Consequently, many semi-supervised frameworks seek supervisory information from alternative sources rather than relying solely on AU labels. Zhang et al. (2019) proposed a context-aware attention mechanism for joint AU intensity estimation, but its application is limited to

a specific dataset. Cui et al. (2020) introduced a constraint optimization method encoding prior knowledge on expression-AU probabilistic dependencies into a Bayesian Network, promoting the generalization ability across different datasets. Chang and Wang (2022) utilized AU labeling rules defined by the Facial Action Coding System to devise a knowledge-driven self-supervised representation learning framework for AU detection.

In contrast to the aforementioned methods, our framework introduces an AU domain separation and reconstruction framework, facilitating the transfer of AU knowledge from the source domain to the target domain. This approach offers adaptability to various domains related to the task and can be widely implemented on static datasets.

2.2. AU domain separation and reconstruction

The AU domain separation and construction represents a prevalent method for transferring knowledge between source and target domains. A common strategy involves employing an adversarial loss with a domain discriminator to render the features of both domains indistinguishable. Ganin et al. (2016) introduced the Domain-Adversarial Neural Network, a shared network facilitating the learning of domain-invariant features. In contrast, Tzeng et al. (2017) proposed the Adversarial Discriminative Domain Adaptation method, pre-training a network on the source domain and refining it on the target domain to minimize adversarial loss between fixed source-domain features and trainable target-domain features. Despite the effectiveness of these methods in domain separation and construction, enforcing feature domain invariance proves impractical for AU detection due to the potential removal of AU-related information intertwined with head poses, causing domain gaps.

An alternative involves translating source images into target-style images. Zheng et al. (2018) presented a method translating rendered images into the real image domain, incorporating identity mapping regularization for real input images. Lee et al. (2018) separated representations for translating images by embedding them into a specialized attribute space for a specific domain and a content space that remains invariant across domains, capturing shared information. Wang and Wang (2018) utilized a generative adversarial network (Goodfellow et al., 2014) to synthesize images resembling the target image while retaining AU patterns from the source image. This approach represents a pioneering effort in AU detection via AU domain separation and construction. However, limitations arise as the processed source and target images exhibit similar expressions and are both constrained, focusing solely on the image differences of AU patterns. Style translation struggles to adequately address gaps between constrained and unconstrained domains, such as occlusion differences.

Additionally, Shao et al. (2022) proposed an end-to-end unconstrained facial AU detection framework based on domain adaptation, transferring accurate AU labels from a constrained source domain to an unconstrained target domain by leveraging AU-related facial landmarks. However,

obtaining a substantial amount of accurate facial landmark ground truths during the training process, particularly in the target domain, proves highly impractical.

In comparison, our method advocates for an adaptive approach to AU detection by utilizing the AU domain separation and reconstruction framework. This approach effectively tackles additional domain shifts resulting from pose variations and occlusions. At the same time, the accurate facial landmark coordinates in target domain needed in the training process can be generated by the framework itself.

2.3. Multi-task learning frameworks for AU detection

Due to the correlation between different facial tasks, deep multi-task learning has been widely used in this field. Firstly, facial landmarks are closely related to AUs, as the former can be used to predefine the positions of AUs. Therefore, there have been many AU detection frameworks based on facial landmark detection. Shao et al. (2021) were the first in amalgamating AU detection and facial landmark detection, leveraging the inherent similarities between these tasks to bolster performance in each. Wang et al. (2023) introduced an innovative multi-task dual learning framework aimed at concurrently executing facial landmark detection and AU recognition, capturing the relationships between facial landmarks and AUs at both the feature and label levels.

In addition, certain AU detection frameworks utilize facial landmarks to localize crucial facial regions and extract local features relevant to AUs. Li et al. (2017) proposed a deep learning framework for AU detection incorporating region of interests (ROIs) adaptation, integrated multi-label learning, and optimal LSTM-based temporal fusing. Li et al. (2017) improved and cropped ROIs with roughly extracted facial landmark information for AU detection. Yang et al. (2023) combined basic facial features, attention-based landmark features, and contrastive learning to enhance AU detection performance.

Furthermore, several frameworks are often integrated with downstream tasks of AU detection, such as facial expression recognition, facial attribute detection and stuff like that. Tallec et al. (2022) introduced a multi-task learning approach incorporating task order optimization and prediction for simultaneous detection of facial attributes and AUs. Zhou and Zhi (2022) developed a multi-task-based facial analysis system integrating various facial attributes, including facial landmarks, head pose, gender, and emotion. Zhou and Zhi (2022) proposed a meta auxiliary learning method that automatically selects highly related facial expression samples by learning adaptive weights for the training facial expression samples in a meta-learning fashion.

Motivated by these methodologies, we have undertaken a novel approach by combining AU domain separation and reconstruction with facial landmark detection for AU detection. Notably, this integration of tasks represents an innovative direction that has not been explored previously.

3. Our Proposed Method

3.1. Overview

Fig. 2 shows the overall architecture of our proposed multi-task learning model, which is consisted of three branches: two facial landmark detection branches, and an AU domain separation and reconstruction branch.

Initially, we begin the training of both facial landmark detection branch in source domain and in target domain with two images I_s and I_t to get 49 facial landmark coordinates in both source domain and target domain and pretraining models for two facial feature extractors $E_f(I_s, F_s)$ and $E_f(I_t, F_t)$. After these two branches have been pre-trained, the source image I_s and the target image I_t are put into the domain separation and reconstruction branch to get AU features F_s and F_t . $E_f(I_s, F_s)$ and $E_f(I_t, F_t)$ will be loaded by initialized parameters from the modules of two facial landmark detection branches. After that, three branches are trained simultaneously.

The AU domain separation and reconstruction branch is consisted of two branches, a source domain branch and a target domain branch. Each branch is separated and reconstructed twice. After putting two images I_s and I_t into $E_f(I_s, F_s)$ and $E_f(I_t, F_t)$, we get two initial facial features F_s and F_t . Then, facial texture encoders $E_l(F_s, F_{sl})$, $E_l(F_t, F_{tl})$ and a background feature generator $G_b(F_s, F_{sb})$, $G_b(F_t, F_{tb})$ are used to separate F_s and F_t into landmark-related features F_{sl} and F_{tl} , and background features F_{sb} and F_{tb} . As shown in Fig. 2, the acquisitions of landmark-related features F_{sl} and F_{tl} are supervised by facial landmark labels FL_s and FL_t from the training of facial landmark detection branches in source domain and target domain, which make our framework become an end-to-end trainable one. A minimax game theory is also employed in the process of feature separation while generators $G_b(F_s, F_{sb})$ and $G_b(F_t, F_{tb})$ attempt to generate background features F_{sb} and F_{tb} , while discriminators $D_l(F_{sb})$ and $D_l(F_{tb})$ aim to detect landmark-related features in F_{sb} and F_{tb} . After that, generators $G_{st}(F_{sb}, F_{sbt})$ and $G_{st}(F_{tb}, F_{tbt})$ are applied to generate new reconstructed features F_{sbt} and F_{tbt} by mixing F_{sl} and F_{tb} , F_{sb} and F_{tl} together. Discriminators $D_d(F_{sbt})$ and $D_d(F_{tbt})$ are used to recognize generated features from other domains. Finally, another round of domain separation and reconstruction which is the same as the first round is introduced to F_{sbt} and F_{tbt} to obtain cross-cyclically reconstructed original features F'_s and F'_t .

Apart from that, we propose a pixel-level feature alignment scheme. To better realize the reconstruction process, we introduce projectors $P(\cdot)$ with simple structure and an improved self-reconstruction loss L_{sr} . Projectors $P(\cdot)$ first amplify the receptive field of feature pixel elements by increasing the depth of neural networks, then L_{sr} aligns similar features from separated and reconstructed process pixel by pixel. Different from the original self-reconstruction loss (Shao et al., 2022; Bhattacharya et al., 2020) with only two pairs of restored features F'_s , F_s and F'_t and F_t , L_{sr} is now working on six pairs of features after adding four

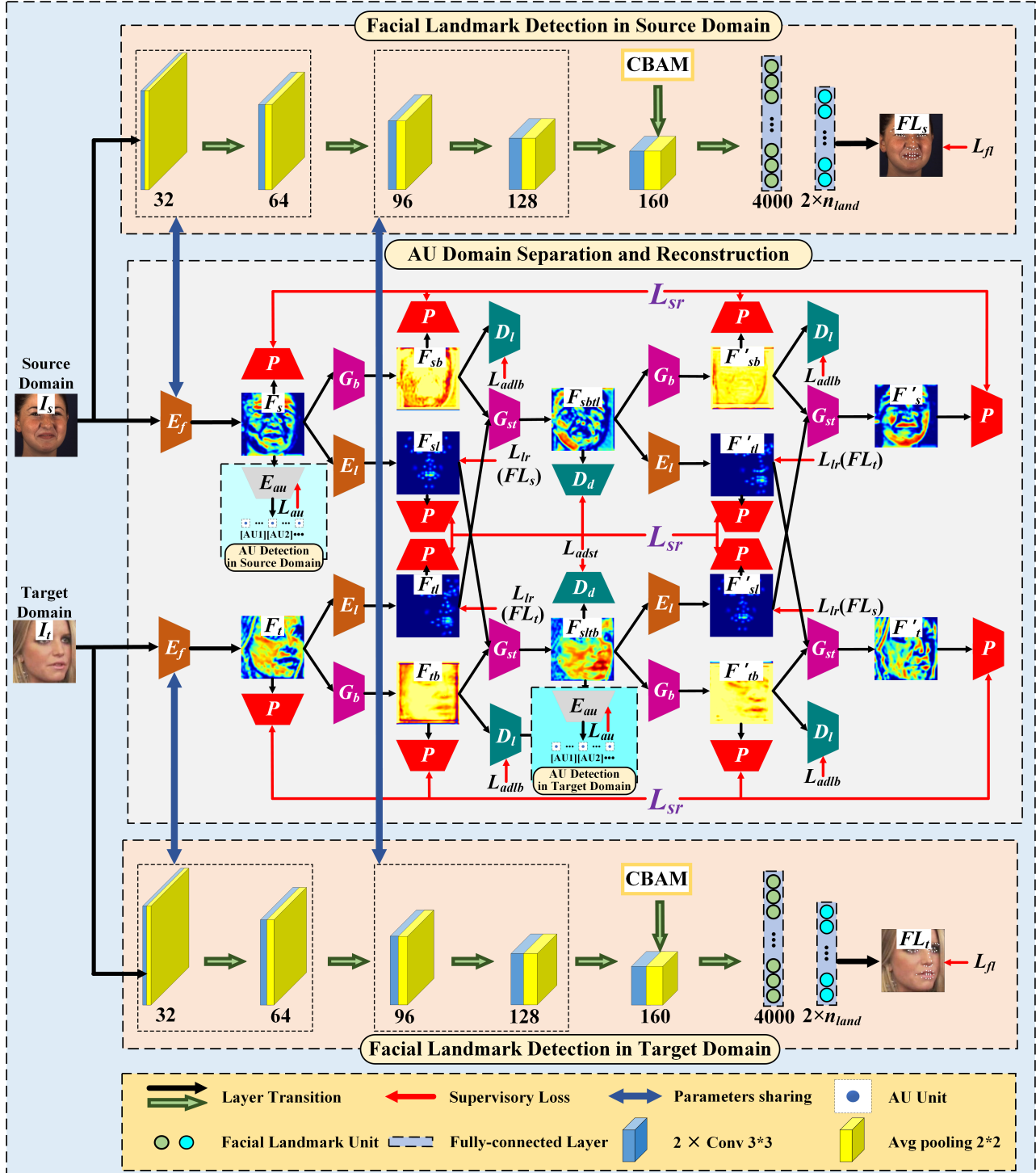


Figure 2: The overall architecture of our proposed multi-task learning model. For AU detection in source domain and target domain, we jointly learn two tasks named AU separation and reconstruction and facial landmark detection to solve the problem of insufficient labels in the wild and weak generalization performance in laboratory scenes. The same features and modules that have the same structure are marked by the same color, and parameters of G_b , E_l , G_{st} , D_l , E_{au} and P are shared by source-domain and target-domain input images.

pairs of intermediate supervisors F'_{sl} and F_{sl} , F'_{sb} and F_{sb} , F'_{lt} and F_{lt} , F'_{tb} and F_{tb} . This makes reconstructed features much closer to original ones, increasing the accuracy of AU detection.

The AU feature extractors $E_{au}(F_s)$ and $E_{au}(F_{stb})$ are trained for AU detection from source domain and target domain, which essentially rely on a semi-supervised learning framework supervising images from both source domain and

target domain by using only AU labels from source domain. This domain adaptive method is also useful to other facial tasks such as facial expression recognition or analysis. More details will be introduced in the following.

3.2. Multi-task learning strategy

As shown in Fig. 2, our proposed AU detection framework adopts the multi-task learning strategy, jointly learning with both AU domain separation and reconstruction task and facial landmark detection. We introduce two facial landmark detection branches from both source domain and target domain to solve the problem of insufficient facial landmark labels when obtaining landmark-related features in AU domain separation and reconstruction branch. This dual domains facial landmark detection framework can also replace ground truths from other facial toolkits with our training facial landmark labels, which avoids the situation that it is unable to get high-precision landmarks in real scenario. Another advantage of this approach is that it enables weight sharing of partial modules among three facial tasks with similar facial features, which can mutually guide each other during training.

The training strategy consists of two stages. The first stage is training two facial landmark detection branches. Each branch comprises five integral modules and two fully-connected layers. For each module, there are two 3×3 convolutional layers with a stride of 1 and padding of 1, followed by a 2×2 average-pooling layer. The channels of convolutional layers in five modules are respectively 32, 64, 96, 128 and 160. After that, the CBAM (Woo et al., 2018) module is appended to the last integral module. At the end of the branch, two fully-connected layers predict facial landmarks trained by L_{fl} as

$$L_{fl}(y, \hat{y}) = -\frac{1}{2s^2} \sum_{i=1}^{n_{land}} [(y_{2i-1} - \hat{y}_{2i-1})^2 + (y_{2i} - \hat{y}_{2i})^2], \quad (1)$$

where y_{2i-1} and y_{2i} represent the actual x-coordinate and y-coordinate of the i-th facial landmark, while \hat{y}_{2i-1} and \hat{y}_{2i} represent the corresponding predicted values. The term n_{land} denotes the total number of facial landmarks, and s represents the inter-ocular distance of two eyes used for normalization.

After the training of two facial landmark detection branches, we separately put both the source image I_s and the target image I_t into two feature extraction modules $E_f(I_s, F_s)$ and $E_f(I_t, F_t)$ with initialized parameters provided by the first two integral modules of two facial landmark detection branches, since $E_f(I_s, F_s)$ and $E_f(I_t, F_t)$ have the same structures as the two integral modules. Then we train three branches, including two facial landmark detection branches and an AU domain separation and reconstruction branch simultaneously. In addition, the third and fourth integral modules of two facial landmark detection branches also share parameters during the whole training process. The advantage of this way is that the number of weight updates that must be carried out in the process of backpropagation

is reduced, and the generalization performance of modules from different domains can be improved by mutually guiding each other during training. Furthermore, the initialized pretraining parameters for facial feature extraction also help $E_f(I_s, F_s)$ and $E_f(I_t, F_t)$ warm up before training, which are able to promote the feature separation process.

3.3. AU Domain Feature Separation and Reconstruction

The AU domain feature separation and reconstruction process contains two branches: the source domain branch and the target domain branch. Each branch is separated and reconstructed twice. Therefore, for the convenience of expression, we only take the target domain branch as an example to explain the whole AU domain feature separation and reconstruction process.

To begin with, our goal is to isolate the initial facial feature F_t into two features, the landmark-related feature F_{tl} and the background feature F_{tb} . The former one includes the inner-landmark information and the latter one excludes the facial inner-landmark information. Due to the fact that adversarial learning based on cross entropy loss (Goodfellow et al., 2014) is widely used for feature separation, we first convert the facial landmark detection task from a regression task (Zhang et al., 2015; Shao et al., 2020) into a classification task (Honari et al., 2016; Xiao et al., 2016) to get F_{tb} . To be more specific, we transform the square feature map of each landmark with a size of $d \times d \times 1$ into independent an one-hot coding sequence with a size of $d^2 \times 1$, since each position on the square feature map is regarded as a binary classification problem. In this multi-label binary classification problem, only the sample of the facial landmark position is a positive one. d represents the side length of the square feature map and d^2 is the length of the one-hot coding sequence. We assume that p_{2i}^t and p_{2i-1}^t are the coordinates of the i-th facial landmark and y_i^t is the index of the facial landmark position in the one-hot coding sequence after transformation. The transformation is defined as

$$y_i^t = (\lfloor p_{2i}^t \cdot d / l \rfloor - 1) \cdot d + \lfloor p_{2i-1}^t \cdot d / l \rfloor, \quad (2)$$

where the notation $\lfloor \cdot \rfloor$ denotes the operation of taking a largest integer not greater than the number. l represents the crop size of the input image I_t . The ground truth is assigned a value of 1 at the facial landmark position and 0 at all other positions.

By regarding the facial landmark detection as a multi-label binary classification problem, we utilize facial texture encoder E_l for extracting landmark-related feature:

$$L_{lr}(E_l, F_t, F_{tl}) = \mathbb{E}_{f^t \sim F_t} \left[\frac{1}{n} \sum_{i=1}^n \sum_{k=1}^{d^2} \mathbb{1}_{[k=y_i^t]} \log(\sigma(E_l^{(i,k)}(f^t))) \right], \quad (3)$$

where f^t is the random variable subject to the distribution of F_t . $E_l^{(i,k)}(\cdot)$ represents the k-th value in the square feature map of the i-th landmark, $\mathbb{1}_{[\cdot]}$ is the indicator function, and

$\sigma(\cdot)$ represents the softmax function. The significance of Eq.(3) is to encourage $E_l(F_t, F_{tl})$ to have the highest value $\sigma(E_l^{(i,k)}(f^t))$ at the position $(\lfloor p_{2i-1}^t \cdot d/l \rfloor, \lfloor p_{2i}^t \cdot d/l \rfloor)$ while having no value at other positions. To make the landmark-related feature F_{tl} include facial landmark information, we can formalize F_{tl} as $\bigoplus_{i=1}^n \sigma(E_l^{(i)}(f^t))$, where \oplus represents the per-pixel addition.

To generate background features without facial landmark information, we introduce the multi-label minimax game theory into the feature separation process, which is also a kind of adversarial learning. Specifically, we train $D_l(F_{tb})$ by minimizing

$$\mathbb{E}_{f^t \sim F_t} \left[\frac{1}{nd^2} \sum_{i=1}^n \sum_{k=1}^{d^2} (\mathbb{1}_{[k \neq y_i^t]} \| D_l^{(i,k)}(G_b(f^t)) \|_2^2 + \mathbb{1}_{[k=y_i^t]} \| D_l^{(i,k)}(G_b(f^t)) - 1 \|_2^2) \right], \quad (4)$$

where the function of $D_l^{(i,k)}(\cdot)$ is similar to $E_l^{(i,k)}(\cdot)$. We encourage $D_l(F_{tb})$ to distinguish 1 at the facial landmark position, while it distinguishes 0 at all other positions. On the contrary, we train G_b by minimizing

$$\mathbb{E}_{f^t \sim F_t} \left[\frac{1}{nd^2} \sum_{i=1}^n \sum_{k=1}^{d^2} \| D_l^{(i,k)}(G_b(f^t)) - \frac{1}{d^2} \|_2^2 \right], \quad (5)$$

where G_b try its utmost to generate background feature F_{tb} , while $D_l(F_{tb})$ is designed to assign a uniform detection probability of $1/d^2$ to all potential facial landmark locations. The multi-label minimax game theory of adversarial learning plays an important role for generating background feature F_{tb} . The facial landmark adversarial loss L_{adlb} is defined as

$$L_{adlb}(G_b, D_l, F_t, F_{tb}) = \mathbb{E}_{f^t \sim F_t} \left[\frac{1}{n} \sum_{i=1}^n \sum_{k=1}^{d^2} \mathbb{1}_{[k=y_i^t]} \log(\sigma(D_l^{(i,k)}(G_b(f^t)))) \right], \quad (6)$$

where $G_b(f^t) = F_{tb}$. L_{adlb} is a kind of multi-class cross entropy loss.

We want to get generating feature F_{sltb} that both have AU labels and a background from target domain. To encourage F_{sltb} to be indistinguishable from other features whose backgrounds are from target domain, we introduce another adversarial loss L_{adst} for the generation of F_{sltb} :

$$L_{adst}(E_l, G_b, G_{st}, D_d, F_t, F_{sltb}) = \mathbb{E}_{f^t \sim F_t} [\log D_d(f^t)] + \mathbb{E}_{f^{sltb} \sim F_{sltb}} [\log(1 - D_d(f^{sltb}))]. \quad (7)$$

To achieve stable feature reconstruction, we use the least-squares loss for L_{adst} . Specially, we train D_d by minimizing $\mathbb{E}_{f^t \sim F_t} [\| D_d(f^t) - 1 \|_2^2] + \mathbb{E}_{f^{sltb} \sim F_{sltb}} [\| D_d(f^{sltb}) \|_2^2]$, and train G_{st} by minimizing $\mathbb{E}_{f^{sltb} \sim F_{sltb}} [\| D_d(f^{sltb}) - 1 \|_2^2]$. The generator G_{st} is applied to generate new reconstructed features F_{sltb} from target domain and the discriminator D_d is used to recognize generated features which are not from target domain.

3.4. Pixel-level Feature Alignment scheme

To maintain the consistency of features obtained from two separation and reconstruction processes, we propose a pixel-level feature alignment scheme, which is realized by 12 projectors $P(F_s)$, $P(F_t)$, $P(F_{sl})$, $P(F_{tl})$, $P(F_{sb})$, $P(F_{tb})$, $P(F'_s)$, $P(F'_t)$, $P(F'_{sl})$, $P(F'_{tl})$, $P(F'_{sb})$, $P(F'_{tb})$ with simple structure and an improved self-reconstruction loss L_{sr} . Specifically, four pairs of intermediate supervisors F'_s and F_{sl} , F'_{sb} and F_{sb} , F'_{tl} and F_{tl} , F'_{tb} and F_{tb} are added to L_{sr} comparing to the original self-reconstruction loss (Shao et al., 2022; Bhattacharya et al., 2020) with only two pairs of restored features F'_s , F_s and F'_{tb} and F_t . The self-reconstruction loss mainly refer to the thought of contrastive learning loss, which utilize L_1 loss with strong robustness:

$$L_c = \frac{1}{h_s \times w_s} \sum_{h_s, w_s} \| F'_s - F_s \| + \frac{1}{h_{sl} \times w_{sl}} \sum_{h_{sl}, w_{sl}} \| F'_{sl} - F_{sl} \| + \frac{1}{h_{sb} \times w_{sb}} \sum_{h_{sb}, w_{sb}} \| F'_{sb} - F_{sb} \| + \frac{1}{h_t \times w_t} \sum_{h_t, w_t} \| F'_t - F_t \| + \frac{1}{h_{tl} \times w_{tl}} \sum_{h_{tl}, w_{tl}} \| F'_{tl} - F_{tl} \| + \frac{1}{h_{tb} \times w_{tb}} \sum_{h_{tb}, w_{tb}} \| F'_{tb} - F_{tb} \|, \quad (8)$$

where h and w denote the spatial locations of each features. Although L_1 loss is simple in form, it is very sensitive to large errors between the predicted value and the actual value. Each projector $P(\cdot)$ is used to amplify the receptive field of feature pixel elements by a relatively simple structure, which is consisted of a 3×3 convolutional layer between two 1×1 convolutional layer with a stride of 1 and padding of 1. These projectors are also efficient enough to ensure accurate alignment and match the dimensions between each pairs of similar facial features. In fact, this simple loss has already been utilized before (Chen et al., 2022; Adriana et al., 2015; Yang et al., 2020), but we are actually trying to reveal the potential value of the additional intermediate supervisions rather than designing a complicated loss for feature alignment. The advantage of this approach is that it achieves pixel-by-pixel alignment of the face-background features and the four additional intermediate supervisions greatly improve the reconstruction process.

3.5. Facial AU detection

The AU detection loss is employed to detect F_s , which represents the initial AU features from source domain, as well as F_{sltb} , which refers to the reconstructed AU feature mixing landmark-related feature F_{sl} from source domain and background feature F_{tb} from target domain together. Traditional supervised AU detection methods use the weighted multi-label cross entropy loss (Shao et al., 2021; Shang et al., 2023) for AU detection. However, we find that AU labels in BP4D and DISFA are very imbalanced. For most AUs, the number of negative samples is much larger than the number of positive ones. To solve this problem of multi-label binary classification with imbalanced samples, we propose a weighted asymmetric loss L_{au} to calculate the values

between ground-truth occurrence values and predicted occurrence probabilities generated by $E_{au}(F_s)$ and $E_{au}(F_{slb})$, which is formulated as

$$L_{au}(y, \hat{y}) = -\frac{1}{n_{au}} \sum_{i=1}^{n_{au}} w_i [y_i \log \hat{y}_i + (1 - y_i)(\hat{y}_i)^\beta \log(1 - \hat{y}_i)], \quad (9)$$

where y_i represents the ground-truth occurrence value (0 or 1) of the i -th AU. The corresponding predicted occurrence probability is denoted as \hat{y}_i . The weight w_i is calculated as $w_i = \frac{(1/r_i)n_{au}}{\sum_{i=1}^{n_{au}} (1/r_i)}$, which is used to ensure balanced training.

It permits reducing the impact of loss values associated with those AUs that are more commonly activated in the training set. Consequently, loss values arising from less frequently inactivating AUs are given greater significance during the training process. r_i represents the occurrence frequency of the i -th AU, and n_{au} is the total number of AUs.

Inspired by the asymmetric loss (Ridnik et al., 2021; Luo et al., 2022), we add the expression $(\hat{y}_i)^\beta$ at the center of $(1 - y_i)(\hat{y}_i)^\beta \log(1 - \hat{y}_i)$ to diminish the impact of loss values arising from inactivated AUs that are easily identifiable, since their predicted probabilities of occurrence \hat{y}_i are close to zero ($\hat{y}_i \ll 0.5$). This adjustment directs the training process to emphasize activated AUs, and inactivated AUs which are difficult to be detected accurately. Additionally, we introduce a hyperparameter β . For the negative samples ($y_i = 0$),

$$\mathcal{L} = (\hat{y}_i)^\beta \log(1 - \hat{y}_i), \quad (10)$$

where \mathcal{L} represents the classification loss of a single AU class, so the gradient is

$$\frac{\partial \mathcal{L}}{\partial \hat{y}_i} = \beta(\hat{y}_i)^{\beta-1} \log(1 - \hat{y}_i) - (\hat{y}_i)^\beta \frac{1}{1 - \hat{y}_i}. \quad (11)$$

Due to the encoder parameter update formula is

$$\theta^{t+1} = \theta^t - \alpha \cdot \frac{\partial \mathcal{L}}{\partial \hat{y}_i} \cdot \frac{\partial \hat{y}_i}{\partial \theta}, \quad (12)$$

where θ is a parameter of our network and α is the learning rate. We can know that β is able to control the gradient magnitude of negative samples, thereby controlling the impact of negative samples on parameters learning.

Combining all the losses, we yield the overall loss

$$L_{all} = \lambda_{lr} L_{lr} + \lambda_{adlb} L_{adlb} + \lambda_{adst} L_{adst} + \lambda_{au} L_{au} + \lambda_{fl} L_{fl} + \lambda_{sr} L_{sr}, \quad (13)$$

where the hyperparameters $\lambda_{(.)}$ are utilized to control the relative significance of each loss term in our proposed multi-task learning strategy. Moreover, Eq. (13) is used for both the source domain and the target domain, and the parameters of modules with the same structure in each domain are shared. It is important to note that our framework is designed to be trainable in an end-to-end manner. This implies that all network modules are simultaneously trained in a joint optimization process, ensuring a comprehensive and integrated learning approach.

Table 1

AU occurrence rates (%) of source-domain training datasets. “-” denotes the dataset does not contain this AU. AUs with occurrence rates larger than 7% are marked in bold.

Dataset	AU Index									
	1	2	4	5	6	9	12	17	25	26
BP4D	18.4	14.6	19.8	3.3	44.0	5.7	54.0	34.2	-	-
DISFA	4.3	3.6	12.2	0.8	7.2	3.1	12.9	4.4	26.2	8.8

4. Experiments

4.1. Experiment Settings

4.1.1. Datasets

In our experiments, we totally utilize three widely-used datasets for AU detection. For the supervised source domain, we utilize BP4D (Zhang et al., 2014) and DISFA (Mavadati et al., 2013). For the unsupervised target domain, we utilize EmotioNet (Fabian Benitez-Quiroz et al., 2016).

BP4D (Zhang et al., 2014) contains 41 participants from 23 females and 18 males. Each person is involved in 8 sessions captured with both 2D and 3D videos. There are about 140,000 frames with AU labels of occurrence or nonoccurrence. Each frame is also annotated with 68 landmarks detected by SDM (Xiong and De la Torre, 2013).

DISFA (Mavadati et al., 2013) consists of 27 videos recorded from 15 men and 12 women. Each video has 4,845 frames and the total number of images is 130,788. The frames are annotated with AU intensities from 0 to 5 and 68 landmarks detected by AAM (Cootes et al., 2001). The frames with intensities equal or greater than 2 are considered as positive, while others are treated as negative.

EmotioNet (Fabian Benitez-Quiroz et al., 2016) is a dataset containing approximately one million training and validation images that are collected from the Internet. AU labels for the validation images are manually annotated by certified experts. The facial toolkit dlib (King, 2012) is used to annotate all 68 landmarks, and any images without detected landmarks are subsequently excluded from the dataset. We randomly select 200,000 training images as the training set and split the validation images into a validation set (10,544 images) and a test set (10,544 images).

For all datasets, we employ a three-fold cross-validation methodology for rigorous evaluation.

4.1.2. Implementation Details

Firstly the 68 facial landmarks are transformed into 49 facial internal landmarks, excluding the facial contour landmarks. Then images are augmented through similarity transformation including in-plane rotation, uniform scaling, and translation using 49 facial landmarks to the same resolution of 200×200×3 pixels, and randomly cropped into $l \times l \times 3$ pixels with random horizontal flip. In our experimental setup, the crop size l and the side length d of square feature map are set to 176 and 44.

Table 2

F1-score of our target domain results and state-of-the-art methods on EmotioNet, where the source domain dataset is BP4D.

Training strategy	Method	AU Index						Avg.
		1	2	4	6	12	17	
Self-supervised learning	ADDA (Tzeng et al., 2017)	17.7	5.2	15.3	38.2	58.7	6.2	23.6
	DANN (Ganin et al., 2016)	16.8	12.7	25.8	28.9	62.5	9.5	26.0
	T²Net (Zheng et al., 2018)	9.4	9.6	24.4	45.1	69.5	4.7	27.1
	DRIT (Lee et al., 2018)	20.4	7.7	30.9	44.2	67.5	8.3	29.8
	ADLD (Shao et al., 2022)	19.8	25.2	31.0	58.2	78.3	8.6	36.8
	Ours	24.3	24.1	36.6	71.5	81.1	13.0	41.8
Pseudo-labels supervised learning	WSC-P (Zhao et al., 2018)	22.7	16.5	39.3	55.2	83.4	10.8	38.0
	JAA-Net-P (Shao et al., 2021)	21.3	19.2	43.6	59.3	85.2	9.3	39.7
	ARL-P (Shao et al., 2019)	22.3	17.4	48.1	57.5	84.6	11.9	40.3
	ADLD-P (Shao et al., 2022)	30.7	26.1	48.1	60.7	77.6	11.5	42.4
	Ours-P	34.2	26.5	49.4	67.4	79.7	17.1	45.7

Table 3

F1-score of our target domain results and state-of-the-art methods on EmotioNet, where the source domain dataset is DISFA.

Training strategy	Method	AU Index					Avg.
		4	6	12	25	26	
Self-supervised learning	T²Net (Zheng et al., 2018)	23.0	37.9	61.6	80.9	28.0	46.3
	DRIT (Lee et al., 2018)	38.0	49.0	64.4	76.4	19.2	49.4
	ADLD (Shao et al., 2022)	27.0	51.8	73.8	88.4	34.2	55.0
	Ours	39.9	64.5	65.4	89.5	27.8	57.4
Pseudo-labels supervised learning	JAA-Net-P (Shao et al., 2021)	47.0	59.7	85.6	88.1	34.4	62.9
	ARL-P (Shao et al., 2019)	52.5	59.6	86.1	89.0	35.5	64.5
	ADLD-P (Shao et al., 2022)	49.5	63.6	86.8	88.6	38.3	65.3
	Ours-P	49.8	67.4	87.6	91.2	42.0	67.6

For the training process, we first simultaneously pretrain two facial landmark detection branches using Adam (Kinga et al., 2015) optimizer. We set $\beta_1 = 0.9$, $\beta_2 = 0.999$, an initial learning rate of 0.001, a weight decay of 0.0005, a batch size of 8 and 20 epochs. The learning rate decays per 10 epochs, which is up to 0.5 of the original. Secondly, pre-training parameters are respectively loaded to two feature extractors $E_f(I_s, F_s)$ and $E_f(I_t, F_t)$. We train the whole multi-task learning model using Adam optimizer for up to 12 epochs. For two facial landmark detection branches, we keep the learning rate of 0.0005. For G_b , G_{st} , D_l and D_d , we set $\beta_1 = 0.5$, $\beta_2 = 0.9$ and a learning rate of 0.00005. For E_f , E_{au} and E_l , we set $\beta_1 = 0.95$, $\beta_2 = 0.999$ and another learning rate of 0.0001. All learning rates remain unchanged during the first 4 epochs and linearly decay during the next 8 epochs. Thirdly, we choose the pre-trained model with the best performance and fine-tune it. To better set appropriate values for the trade-off parameters λ_{lr} , λ_{adlb} , λ_{adst} , λ_{au} , λ_{fl} and λ_{sr} , we use the control variable method to change only one parameter every time and set λ_{lr} , λ_{adlb} , λ_{adst} , λ_{au} , λ_{fl} and λ_{sr} to 0.6, 400, 1.2, 1, 0.1 and 100 respectively by verification experiments. The experimental results of these hyperparameters are shown in Table 7.

4.1.3. Evaluation Metrics

BP4D, DISFA, and EmotioNet collectively contain 17 AU labels (AU 1, AU 2, AU 4, AU 5, AU 6, AU 7, AU 9, AU 10, AU 12, AU 14, AU 15, AU 17, AU 20, AU 23, AU 24, AU 25, AU 26). The descriptions of AU centers and their respective location definitions are the same in ADLD (Shao et al., 2022).

Table. 1 provides a summary of the occurrence rates of different AUs in the training sets of the source domain. There is variation in the occurrence rates of different AUs, with some having low rates while others have high rates. To tackle the problem of data imbalance, our framework evaluation focuses solely on AUs with occurrence rates exceeding 7% in the training set of the source domain. Specifically, for the BP4D dataset, we utilize AUs 1, 2, 4, 6, 12, and 17, while for the DISFA dataset, we consider AUs 4, 6, 12, 25, and 26.

The evaluation metrics of AU detection and facial landmark detection are both shown as follows:

- **AU detection.** Consistent with state-of-the-art approaches, we employed two widely used frame-based metrics for AU detection: F1-score(%) and Accuracy(%). F1-score is the harmonic mean of precision and recall, used the most widely in AU detection. For each method, we compute average metrics over all AUs (denoted as Avg.).

Table 4

F1-score of our source domain results and state-of-the-art methods on BP4D, where the target domain dataset is EmotioNet.

Method	AU Index						Avg.
	1	2	4	6	12	17	
SimCLR (Chen et al., 2020)	38.0	36.4	37.2	66.6	76.2	56.1	51.8
SLTC (Lu et al., 2020)	42.3	24.3	44.1	71.8	83.3	51.6	52.9
SimSiam (Chen and He, 2021)	38.6	39.0	37.2	68.2	77.6	57.9	53.1
Fab-Net (Wiles et al., 2018a)	43.3	35.7	41.6	72.9	83.5	48.2	54.2
MoCo (He et al., 2020)	30.8	41.3	42.1	70.2	82.5	59.1	54.3
CVC (Wu and Wang, 2021)	43.9	47.8	38.7	67.0	84.4	49.3	55.2
EmoCo (Sun et al., 2021)	45.4	30.5	55.5	76.1	87.6	59.1	59.0
ADLD (Shao et al., 2022)	50.5	35.7	61.8	74.1	75.2	69.0	61.0
TAE (Li et al., 2022)	47.0	45.9	50.9	74.7	85.6	62.3	61.1
CLP (Li and Shan, 2023)	47.7	50.9	49.5	75.8	84.1	62.7	61.8
KSRL (Chang and Wang, 2022)	50.1	45.4	53.6	79.2	87.4	56.1	62.0
Ours	52.9	38.0	61.4	77.9	77.2	71.9	63.2

Table 5

F1-score of our source domain results and state-of-the-art methods on DISFA, where the target domain dataset is EmotioNet.

Method	AU Index					Avg.
	4	6	12	25	26	
SLTC (Lu et al., 2020)	35.1	33.6	67.5	68.0	43.8	49.6
Fab-Net (Wiles et al., 2018a)	43.2	50.4	69.6	72.4	42.4	55.6
SimCLR (Chen et al., 2020)	47.5	42.4	66.8	81.5	52.7	58.2
MoCo (He et al., 2020)	45.9	45.4	72.9	83.4	54.5	60.2
CVC (Wu and Wang, 2021)	56.4	49.5	75.5	79.1	55.7	64.2
EmoCo (Sun et al., 2021)	63.9	52.5	77.0	78.3	44.2	63.2
SimSiam (Chen and He, 2021)	58.1	53.8	74.4	79.0	55.7	64.2
TAE (Li et al., 2022)	64.5	46.8	73.2	85.1	55.3	65.0
KSRL (Chang and Wang, 2022)	58.1	52.5	77.6	86.9	53.2	65.7
Ours	65.2	40.2	74.3	88.6	60.9	65.8

- Facial landmark detection. For this task, we use both Mean error (%) and Failure rate (%). The mean error of more than 10% is considered unqualified.

4.2. Comparison with State-of-the-Art Methods

We evaluate our approach against current state-of-the-art methods, including AU detection in target domain methods, AU detection in source domain methods and facial landmark detection methods.

4.2.1. AU Detection in Target Domain

Due to our framework does not utilize AU labels during the target domain training process, it is essentially a self-supervised learning one. However, to compare with fully-supervised AU detection methods, we introduce AU pseudo labels of the target domain images from facial toolkit OpenFace (Baltrusaitis et al., 2018) in our framework. Specifically, we add another two AU detection branches after F_t and F_{sbt} respectively, supervised by the introduced AU pseudo labels. This also improves the accuracy of AU detection after F_s and F_{sbt} , since the parameters of modules with the same structure of the two branches in AU domain separation and reconstruction process are shared.

We compare our AU detection results without pseudo labels in target domain to traditional adversarial domain adaptation methods, including **ADDA** (Tzeng et al., 2017), **DANN** (Ganin et al., 2016) which learn domain invariant features, and **T²Net** (Zheng et al., 2018), **DRIT** (Lee et al., 2018), **ADLD** (Shao et al., 2022), which transfer the source-style images into target-style images. In addition, the results with pseudo labels are compared with **ADLD** and three fully-supervised AU detection methods **JAA-Net-P** (Shao et al., 2021), **ARL-P** (Shao et al., 2019), **WSC-P** (Zhao et al., 2018). Quantitative results on the target domain dataset EmotioNet when the source domain is BP4D are summarized in Table 2, where our method achieves the best overall performance.

For self-supervised learning frameworks, compared to ADDA and DANN, our method achieves an average increase of 18.2% and 15.8%. This occurs because by enforcing domain invariance of features when feeding them into the AU detector $E_{au}(F_{sbt})$, and essential AU-related information may be overlooked. Compared to T²Net and DRIT, our method outperforms 14.7% and 12.0%. This is attributed to the ability of our approach to overcome the limitations caused by substantial domain shifts, such as variations in

head poses and occlusion distributions, which can negatively impact target-domain AU detection. Furthermore, our method outperforms 5.0% in F1-score to ADLD, which confirms the effectiveness of multi-task learning strategy, feature alignment scheme and weighted asymmetric loss.

For pseudo-labels supervised learning frameworks, compared to JAA-Net-P and ARL-P, our method achieves an average increase of 6.0% and 5.4%. This occurs because the complex fully-supervised AU detection modules need to adjust the optimizer hyperparameters and loss function weights precisely during training, otherwise AU detection accuracy will be affected. However, the structure of our AU detection module $E_{au}(F_{slb})$ is relatively simple. Besides, although WSC-P can refine the inaccurate pseudo AU labels, its results are the worst.

Table. 3 summarizes the results obtained from EmotioNet when the source domain is DISFA. Our method demonstrates superior performance in overall AU detection compared to other approaches.

4.2.2. AU Detection in Source Domain

We compare our AU detection results in source domain to the state-of-the-art advanced self-supervised approaches, including six typical self-supervised AU detection methods **SLTC** (Lu et al., 2020), **Fab-Net** (Wiles et al., 2018a), **TAE** (Li et al., 2022), **EmoCo** (Sun et al., 2021), **ADLD** (Shao et al., 2022), **KSRL** (Chang and Wang, 2022), and five representative contrastive representation learning methods **SimCLR** (Chen et al., 2020), **SimSiam** (Chen and He, 2021), **MoCo** (He et al., 2020), **CVC** (Wu and Wang, 2021), **CLP** (Li and Shan, 2023) in Table. 4 and Table. 5. Although these methods are all based on unsupervised self-supervised frameworks, but they all used AU labels from source domain datasets to verify the experimental results.

The results on BP4D are shown in Table. 4. Although our source domain AU detection network structure is relatively simple, our method achieves an average increase of 10.3%, 9.0%, 4.2%, 2.1% to SLTC, Fab-Net, EmoCo, TAE. This is because these methods only concentrate on global facial features, overlooking task-related domain knowledge such as the distinctive properties of AUs. Compared to contrastive representation learning methods, namely SimCLR, SimSiam, MoCo, CVC and CLP, our method outperforms by around 1.4%-11.4% in F1-score. This occurs because our approach takes full advantage of static datasets, while the prevalent use of self-supervised tasks based on random crops or temporal consistency in contrastive approaches can lead to insufficient AU representations. The reason for the 2.2% improvement over ADLD is that loading pre-training parameters help the initial facial extractor $E_f(I_s, F_s)$ warm up before training. Compared to the second best approach KSRL, our method has demonstrated superior performance by increasing the F1-score from 62.0% to 63.2%. It should be noted that compared with KSRL training in laboratory scene, using backgrounds in the wild greatly improves the generalization performance of our framework.

Table 6

Mean error (lower is better) and failure rate (lower is better) results of different facial landmark detection methods on BP4D.

Method	Mean Error	Failure Rate
MCL (Shao et al., 2020)	7.20	1.69
TCDCN (Zhang et al., 2015)	6.57	1.88
ERT (Kazemi and Sullivan, 2014)	4.73	3.49
LAB (Wu et al., 2018)	4.50	0.11
HRNetV2 (Wang et al., 2020)	4.35	0.02
OpenPose (He et al., 2017)	3.93	0.27
JAA-Net (Shao et al., 2021)	3.80	0.32
Ours(DD only)	5.87	1.16
Ours	3.16	0.19

Similar results can be observed on DISFA as summarized in Table. 5, where our method achieves the best overall AU detection performance.

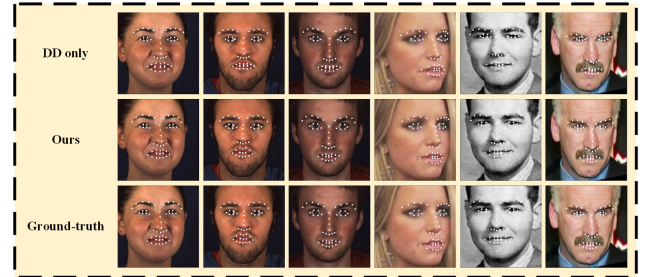


Figure 3: Qualitative results of facial landmark detection in both source domain and target domain.

4.2.3. Comparision with facial landmark detection methods

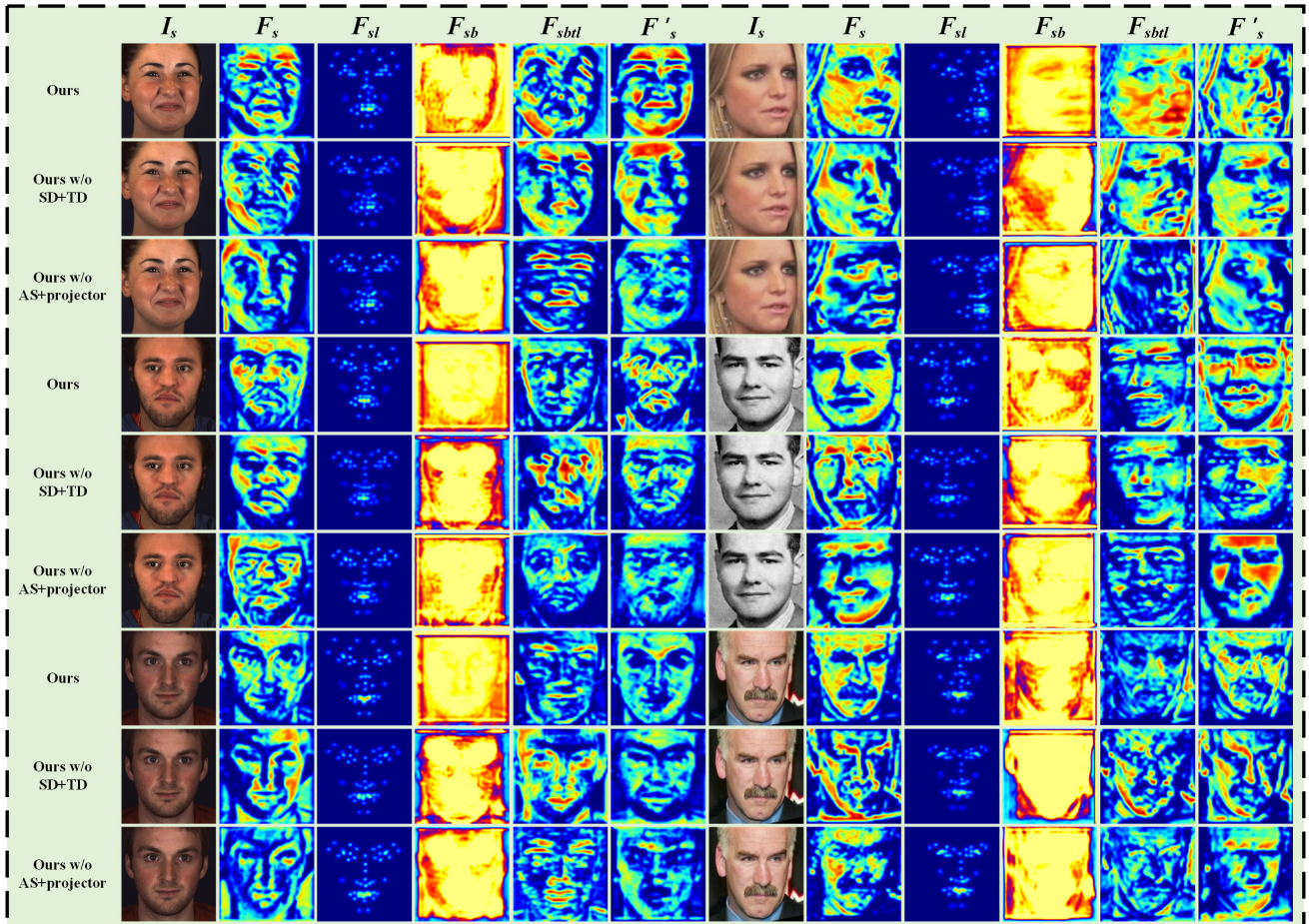
Due to the different ways of obtaining the ground truths of facial landmark detection from target domain dataset EmotioNet, there is no certain standard for evaluating the accuracy facial landmark detection in target domain at present. Table. 6 only shows the mean error and failure rate results of our facial landmark detection framework on BP4D. Additionally, we compare our method with state-of-the-art facial landmark detection methods, including **MCL** (Shao et al., 2020), **TCDCN** (Zhang et al., 2015), **ERT** (Kazemi and Sullivan, 2014), **LAB** (Wu et al., 2018), **HRNetV2** (Wang et al., 2020), **OpenPose** (He et al., 2017), **JAA-Net** (Shao et al., 2021). The qualitative results of facial landmark detection in both source domain and target domain are shown in Fig. 3.

It can be found that our methods exhibit superior performance compared to MCL, TCDCN, ERT, OpenPose, and JAA-Net, excelling in both mean error and failure rate metrics. Notably, despite being specifically tailored for AU detection, our approach outperforms even recently proposed methods such as LAB and HRNetV2 in terms of mean error, showcasing the lowest mean error overall.

Table 7

F1-scores on EmotioNet when the source domain is BP4D for ablation study.

Model	BL	SD	TD	AS	AP	AL	F1-Score	Accuracy
A	✓						36.5	86.4
B	✓	✓					37.5(+1.0)	87.1(+0.7)
C	✓		✓				37.8(+1.3)	87.3(+0.9)
D	✓	✓	✓				38.6(+2.1)	87.6(+1.2)
E	✓	✓	✓	✓			39.0(+2.5)	87.7(+1.3)
F	✓	✓	✓	✓	✓		40.2(+3.7)	88.1(+1.7)
G	✓	✓	✓	✓	✓	✓	41.8(+5.3)	88.5(+2.1)

**Figure 4:** Qualitative results of the ablation studies in both source domain and target domain.

Besides, with the help of AU domain separation and reconstruction task and AU detection task, our method outperforms dual domains facial landmark detection framework (DD) training only with large margins of 2.71% and 0.97% for mean error and failure rate respectively. This demonstrates that other facial tasks are also beneficial for facial landmark detection. These three facial tasks contribute to each other in our proposed multi-task learning strategy.

4.3. Ablation Study

Quantitative results of our framework with different component combinations are summarized in Table. 7, including the baseline (BL), the source domain facial landmark detection (SD), the target domain facial landmark detection (TD), the pixel-level feature alignment scheme (AS), the projectors for alignment (AP) and weighted asymmetric loss (AL).

Contribution of multi-task learning strategy: As summarized in Table. 7, the introduction of dual domains facial landmark detection framework helps achieve an increase of 2.1% in F1-score and 1.2% in Accuracy comparing to the

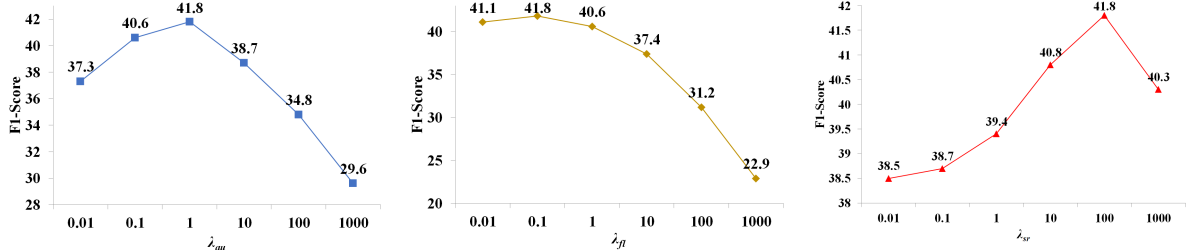


Figure 5: The analysis of hyperparameter $\lambda_{(.)}$ in the overall loss L_{all} .

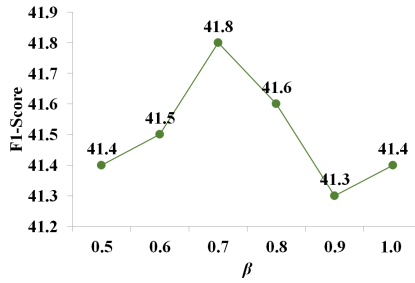


Figure 6: The analysis of hyperparameter β .

baseline, validating that weight sharing of homostructural facial extraction modules can promote the training accuracy of two similar facial tasks. At the same time, the results of two facial landmark detection branches training together exceed the results of one of the branches training alone, which also demonstrate the effectiveness of multi-task learning strategy.

Integrating of pixel-level feature alignment scheme:

The introduction of the pixel-level feature alignment scheme without projectors helps achieve an average increase of 0.4% in F1-score comparing to model D, which illustrates that adding four intermediate supervisors can play a certain role in better feature reconstruction. Moreover, the result of model F sharply increased to 40.2% by adding projectors before reconstructed features, since projectors with simple structures add the number of neural network layers, thus increasing the fitting ability of our framework.

Effectiveness of weighted asymmetric loss: Our proposed weighted asymmetric loss leads to an increase of 1.6% in F1-score comparing to model F by changing the contribution of positive and negative samples of each type of AUs to model parameters updating. This demonstrates that the training process concentrates more on the small number of samples, making the distribution of positive samples have a more significant impact on the binary classification predicting results.

Based on ablation studies, introducing each component is beneficial for performance improvement, among which AL is the most effective component. Qualitative results of the ablation studies are shown in Fig. 4.

4.4. Hyperparameters Analysis

4.4.1. $\lambda_{(.)}$ in the overall loss L_{all}

Due to λ_{lr} , λ_{adtb} , λ_{adst} are fixed to ensure the separation effect, we only vary λ_{au} , λ_{fl} and λ_{sr} from 0.01 to 1000, to investigate its influence on our framework. The experiment results are respectively shown in Fig. 5. We observe that λ_{sr} works best at 100, which illustrates that the improved self-reconstruction loss plays a very important role in the training process. The reason why λ_{fl} should not be large is to avoid convergence of features of two different facial tasks.

4.4.2. Backpropagation rate controller β

As we know, β can control the gradient magnitude of negative samples, so we vary the hyperparameter $\beta = \{0.5, 0.6, 0.7, 0.8, 0.9, 1.0\}$ to find changes of experimental results, which are shown in Fig. 6. We notice that β works best at 0.7, which leads to an increase of 0.4% in F1-score comparing to β on a par with 1.0. This demonstrates that β can help us better control the impact of negative samples on parameters learning

5. Conclusion

In this paper, we propose a multi-task learning strategy boosting AU detection in the wild through jointing facial landmark detection and AU domain separation and reconstruction. Two facial landmark detection branches help solve the lack of accurate facial landmark coordinates during the AU domain separation and reconstruction training process, while the parameters of homostructural facial extraction modules from these two tasks are shared. Apart from that, our proposed pixel-level feature alignment scheme maintains the consistency of features obtained from two separation and reconstruction processes. In addition, the weighted asymmetric loss respectively changes the contribution of positive and negative samples of each type of AUs to model parameters updating. Experimental results demonstrate the superior performance of our framework for AU detection in the wild.

Acknowledgement

The computation is completed in the HPC Platform of Huazhong University of Science and Technology.

CRediT authorship contribution statement

Ziqiao Shang: Methodology, Analysis, Experiment, Manuscript editing. **Bin Liu:** Methodology, Analysis, Manuscript editing.

References

Adriana, R., Nicolas, B., Ebrahimi, K.S., Antoine, C., Carlo, G., Yoshua, B., 2015. Fitnets: Hints for thin deep nets. International Conference on Learning Representations (ICLR) 2, 3.

Baltrusaitis, T., Zadeh, A., Lim, Y.C., Morency, L.P., 2018. Openface 2.0: Facial behavior analysis toolkit, in: 2018 13th IEEE international conference on automatic face & gesture recognition (FG), IEEE. pp. 59–66.

Bauer, A., Wollherr, D., Buss, M., 2008. Human–robot collaboration: a survey. International Journal of Humanoid Robotics 5, 47–66.

Bhattacharya, U., Roncal, C., Mittal, T., Chandra, R., Kapsakis, K., Gray, K., Bera, A., Manocha, D., 2020. Take an emotion walk: Perceiving emotions from gaits using hierarchical attention pooling and affective mapping, in: Proceedings of the European conference on computer vision (ECCV), Springer. pp. 145–163.

Chang, Y., Wang, S., 2022. Knowledge-driven self-supervised representation learning for facial action unit recognition, in: Proceedings of the IEEE/CVF Conference on Computer Vision and Pattern Recognition (CVPR), pp. 20417–20426.

Chen, D., Mei, J.P., Zhang, H., Wang, C., Feng, Y., Chen, C., 2022. Knowledge distillation with the reused teacher classifier, in: Proceedings of the IEEE/CVF Conference on Computer Vision and Pattern Recognition (CVPR), pp. 11933–11942.

Chen, T., Kornblith, S., Norouzi, M., Hinton, G., 2020. A simple framework for contrastive learning of visual representations, in: International conference on machine learning (ICML), PMLR. pp. 1597–1607.

Chen, X., He, K., 2021. Exploring simple siamese representation learning, in: Proceedings of the IEEE/CVF conference on computer vision and pattern recognition (CVPR), pp. 15750–15758.

Cootes, T.F., Edwards, G.J., Taylor, C.J., 2001. Active appearance models. IEEE Transactions on pattern analysis and machine intelligence 23, 681–685.

Corneanu, C., Madadi, M., Escalera, S., 2018. Deep structure inference network for facial action unit recognition, in: Proceedings of the european conference on computer vision (ECCV), pp. 298–313.

Cui, Z., Song, T., Wang, Y., Ji, Q., 2020. Knowledge augmented deep neural networks for joint facial expression and action unit recognition. Advances in Neural Information Processing Systems 33, 14338–14349.

Dahmane, M., Meunier, J., 2014. Prototype-based modeling for facial expression analysis. IEEE Transactions on Multimedia 16, 1574–1584.

Fabian Benitez-Quiroz, C., Srinivasan, R., Martinez, A.M., 2016. Emotionet: An accurate, real-time algorithm for the automatic annotation of a million facial expressions in the wild, in: Proceedings of the IEEE/CVF Conference on Computer Vision and Pattern Recognition (CVPR), pp. 5562–5570.

Ganin, Y., Ustinova, E., Ajakan, H., Germain, P., Larochelle, H., Laviolette, F., March, M., Lempitsky, V., 2016. Domain-adversarial training of neural networks. Journal of machine learning research 17, 1–35.

Goodfellow, I., Pouget-Abadie, J., Mirza, M., Xu, B., Warde-Farley, D., Ozair, S., Courville, A., Bengio, Y., 2014. Generative adversarial nets. Advances in neural information processing systems 27.

He, J., Li, D., Yang, B., Cao, S., Sun, B., Yu, L., 2017. Multi view facial action unit detection based on cnn and blstm-rnn, in: 2017 12th IEEE International Conference on Automatic Face & Gesture Recognition (FG), IEEE. pp. 848–853.

He, K., Fan, H., Wu, Y., Xie, S., Girshick, R., 2020. Momentum contrast for unsupervised visual representation learning, in: Proceedings of the IEEE/CVF conference on computer vision and pattern recognition (CVPR), pp. 9729–9738.

Honari, S., Yosinski, J., Vincent, P., Pal, C., 2016. Recombinator networks: Learning coarse-to-fine feature aggregation, in: Proceedings of the IEEE/CVF Conference on Computer Vision and Pattern Recognition (CVPR), pp. 5743–5752.

Jyoti, S., Sharma, G., Dhall, A., 2018. A single hierarchical network for face, action unit and emotion detection, in: 2018 Digital Image Computing: Techniques and Applications (DICTA), IEEE. pp. 1–8.

Kazemi, V., Sullivan, J., 2014. One millisecond face alignment with an ensemble of regression trees, in: Proceedings of the IEEE conference on computer vision and pattern recognition (CVPR), pp. 1867–1874.

King, D., 2012. Dlib c++ library. Access on: <http://dlib.net>.

Kinga, D., Adam, J.B., et al., 2015. A method for stochastic optimization, in: International conference on learning representations (ICLR), San Diego, California; p. 6.

Lee, H.Y., Tseng, H.Y., Huang, J.B., Singh, M., Yang, M.H., 2018. Diverse image-to-image translation via disentangled representations, in: Proceedings of the European conference on computer vision (ECCV), pp. 35–51.

Li, W., Abtahi, F., Zhu, Z., 2017. Action unit detection with region adaptation, multi-labeling learning and optimal temporal fusing, in: Proceedings of the IEEE conference on computer vision and pattern recognition (CVPR), pp. 1841–1850.

Li, W., Abtahi, F., Zhu, Z., Yin, L., 2018. Eac-net: Deep nets with enhancing and cropping for facial action unit detection. IEEE transactions on pattern analysis and machine intelligence 40, 2583–2596.

Li, Y., Shan, S., 2023. Contrastive learning of person-independent representations for facial action unit detection. IEEE Transactions on Image Processing .

Li, Y., Zeng, J., Shan, S., 2022. Learning representations for facial actions from unlabeled videos. IEEE Transactions on Pattern Analysis and Machine Intelligence 44, 302–317.

Li, Y., Zeng, J., Shan, S., Chen, X., 2019. Self-supervised representation learning from videos for facial action unit detection, in: Proceedings of the IEEE/CVF Conference on Computer vision and pattern recognition (CVPR), pp. 10924–10933.

Liu, Z., Liu, R., Shi, Z., Liu, L., Mi, X., Murase, K., 2023. Semi-supervised contrastive learning with soft mask attention for facial action unit detection, in: IEEE International Conference on Acoustics, Speech and Signal Processing (ICASSP), IEEE. pp. 1–5.

Lu, L., Tavabi, L., Soleymani, M., 2020. Self-supervised learning for facial action unit recognition through temporal consistency, in: British Machine Vision Conference (BMVC), IEEE. pp. 1–8.

Luo, C., Song, S., Xie, W., Shen, L., Gunes, H., 2022. Learning multi-dimensional edge feature-based au relation graph for facial action unit recognition .

Ma, C., Chen, L., Yong, J., 2019. Au r-cnn: Encoding expert prior knowledge into r-cnn for action unit detection. Neurocomputing 355, 35–47.

Mavadati, S.M., Mahoor, M.H., Bartlett, K., Trinh, P., Cohn, J.F., 2013. Disfa: A spontaneous facial action intensity database. IEEE Transactions on Affective Computing 4, 151–160.

McDuff, D., El Kalioubi, R., Demirdjian, D., Picard, R., 2013. Predicting online media effectiveness based on smile responses gathered over the internet, in: 2013 10th IEEE international conference and workshops on automatic face and gesture recognition (FG), IEEE. pp. 1–7.

Niu, X., Han, H., Shan, S., Chen, X., 2019. Multi-label co-regularization for semi-supervised facial action unit recognition. Advances in neural information processing systems 32.

Ridnik, T., Ben-Baruch, E., Zamir, N., Noy, A., Friedman, I., Protter, M., Zelnik-Manor, L., 2021. Asymmetric loss for multi-label classification, in: Proceedings of the IEEE/CVF International Conference on Computer Vision (ICCV), pp. 82–91.

Rosenberg, E.L., Ekman, P., 2020. What the face reveals: Basic and applied studies of spontaneous expression using the Facial Action Coding System (FACS). Oxford University Press.

Shang, Z., Du, C., Li, B., Yan, Z., Yu, L., 2023. Mma-net: Multi-view mixed attention mechanism for facial action unit detection. Pattern Recognition Letters .

Shao, Z., Cai, J., Cham, T.J., Lu, X., Ma, L., 2022. Unconstrained facial action unit detection via latent feature domain. IEEE Transactions on

Affective Computing 13, 1111–1126.

Shao, Z., Liu, Z., Cai, J., Ma, L., 2021. Jaa-net: joint facial action unit detection and face alignment via adaptive attention. International Journal of Computer Vision 129, 321–340.

Shao, Z., Liu, Z., Cai, J., Wu, Y., Ma, L., 2019. Facial action unit detection using attention and relation learning. IEEE transactions on affective computing 13, 1274–1289.

Shao, Z., Zhu, H., Tan, X., Hao, Y., Ma, L., 2020. Deep multi-center learning for face alignment. Neurocomputing 396, 477–486.

Simon, T., Joo, H., Matthews, I., Sheikh, Y., 2017. Hand keypoint detection in single images using multiview bootstrapping, in: Proceedings of the IEEE conference on Computer Vision and Pattern Recognition (CVPR), pp. 1145–1153.

Sun, X., Zeng, J., Shan, S., 2021. Emotion-aware contrastive learning for facial action unit detection, in: 2021 16th IEEE International Conference on Automatic Face and Gesture Recognition (FG), IEEE. pp. 1–8.

Szirtes, G., Szolgyay, D., Utasi, Á., Takács, D., Petrás, I., Fodor, G., 2013. Facing reality: An industrial view on large scale use of facial expression analysis, in: Proceedings of the 2013 on Emotion recognition in the wild challenge and workshop, pp. 1–8.

Tallec, G., Dapogny, A., Baily, K., 2022. Multi-order networks for action unit detection. IEEE Transactions on Affective Computing .

Tzeng, E., Hoffman, J., Saenko, K., Darrell, T., 2017. Adversarial discriminative domain adaptation, in: Proceedings of the IEEE conference on computer vision and pattern recognition (CVPR), pp. 7167–7176.

Vicente, F., Huang, Z., Xiong, X., De la Torre, F., Zhang, W., Levi, D., 2015. Driver gaze tracking and eyes off the road detection system. IEEE Transactions on Intelligent Transportation Systems 16, 2014–2027.

Wang, C., Wang, S., 2018. Personalized multiple facial action unit recognition through generative adversarial recognition network, in: Proceedings of the 26th ACM international conference on Multimedia (ACM MM), pp. 302–310.

Wang, F., Xiang, X., Liu, C., Tran, T.D., Reiter, A., Hager, G.D., Quon, H., Cheng, J., Yuille, A.L., 2017. Transferring face verification nets to pain and expression regression. arXiv preprint arXiv:1702.06925 .

Wang, J., Sun, K., Cheng, T., Jiang, B., Deng, C., Zhao, Y., Liu, D., Mu, Y., Tan, M., Wang, X., et al., 2020. Deep high-resolution representation learning for visual recognition. IEEE transactions on pattern analysis and machine intelligence 43, 3349–3364.

Wang, S., Chang, Y., Wang, C., 2023. Dual learning for joint facial landmark detection and action unit recognition. IEEE Transactions on Affective Computing .

Wiles, O., Koepke, A., Zisserman, A., 2018a. Self-supervised learning of a facial attribute embedding from video, in: British Machine Vision Conference (BMVC), IEEE. pp. 1–15.

Wiles, O., Koepke, A., Zisserman, A., 2018b. X2face: A network for controlling face generation using images, audio, and pose codes, in: Proceedings of the European conference on computer vision (ECCV), pp. 670–686.

Woo, S., Park, J., Lee, J.Y., Kweon, I.S., 2018. Cbam: Convolutional block attention module, in: Proceedings of the European conference on computer vision (ECCV), pp. 3–19.

Wu, H., Wang, X., 2021. Contrastive learning of image representations with cross-video cycle-consistency, in: Proceedings of the IEEE/CVF International Conference on Computer Vision (ICCV), pp. 10149–10159.

Wu, W., Qian, C., Yang, S., Wang, Q., Cai, Y., Zhou, Q., 2018. Look at boundary: A boundary-aware face alignment algorithm, in: Proceedings of the IEEE conference on computer vision and pattern recognition (CVPR), pp. 2129–2138.

Xiao, S., Feng, J., Xing, J., Lai, H., Yan, S., Kassim, A., 2016. Robust facial landmark detection via recurrent attentive-refinement networks, in: Proceedings of the European conference on computer vision (ECCV), Springer. pp. 57–72.

Xiong, X., De la Torre, F., 2013. Supervised descent method and its applications to face alignment, in: Proceedings of the IEEE/CVF Conference on Computer Vision and Pattern Recognition (CVPR), pp. 532–539.

Yan, J., Wang, J., Li, Q., Wang, C., Pu, S., 2021. Self-supervised regional and temporal auxiliary tasks for facial action unit recognition, in: Proceedings of the 29th ACM International Conference on Multimedia (ACM MM), pp. 1038–1046.

Yan, J., Wang, J., Li, Q., Wang, C., Pu, S., 2023. Weakly supervised regional and temporal learning for facial action unit recognition. IEEE Transactions on Multimedia .

Yang, J., Martinez, B., Bulat, A., Tzimiropoulos, G., 2020. Knowledge distillation via softmax regression representation learning, in: International Conference on Learning Representations (ICLR).

Yang, Y., Hu, Q., Lu, H., Jiang, F., Li, Y., 2023. Landmark-assisted facial action unit detection with optimal attention and contrastive learning, in: International Conference on Neural Information Processing (ICONIP), Springer. pp. 92–104.

Zhang, X., Yin, L., Cohn, J.F., Canavan, S., Reale, M., Horowitz, A., Liu, P., Girard, J.M., 2014. Bp4d-spontaneous: a high-resolution spontaneous 3d dynamic facial expression database. Image and Vision Computing 32, 692–706.

Zhang, Y., Jiang, H., Wu, B., Fan, Y., Ji, Q., 2019. Context-aware feature and label fusion for facial action unit intensity estimation with partially labeled data, in: Proceedings of the IEEE/CVF International Conference on Computer Vision (CVPR), pp. 733–742.

Zhang, Z., Luo, P., Loy, C.C., Tang, X., 2015. Learning deep representation for face alignment with auxiliary attributes. IEEE transactions on pattern analysis and machine intelligence 38, 918–930.

Zhao, K., Chu, W.S., Martinez, A.M., 2018. Learning facial action units from web images with scalable weakly supervised clustering, in: Proceedings of the IEEE Conference on computer vision and pattern recognition (CVPR), pp. 2090–2099.

Zhao, K., Chu, W.S., Zhang, H., 2016. Deep region and multi-label learning for facial action unit detection, in: Proceedings of the IEEE conference on computer vision and pattern recognition (CVPR), pp. 3391–3399.

Zheng, C., Cham, T.J., Cai, J., 2018. T2net: Synthetic-to-realistic translation for solving single-image depth estimation tasks, in: Proceedings of the European conference on computer vision (ECCV), pp. 767–783.

Zhou, C., Zhi, R., 2022. Learning deep representation for action unit detection with auxiliary facial attributes. International Journal of Machine Learning and Cybernetics , 1–13.

Zhu, X., Lei, Z., Liu, X., Shi, H., Li, S.Z., 2016. Face alignment across large poses: A 3d solution, in: Proceedings of the IEEE conference on computer vision and pattern recognition (CVPR), pp. 146–155.